Journal of the Meteorological Society of Japan, Vol.79, No.1, pp.161–171, 2001

Logarithmic Relation between the Initial Error and Predictability for the Barotropic Component of the Atmosphere

By Daisuke Nohara and H.L. Tanaka

Institute of Geoscience, University of Tsukuba, Tsukuba, Japan

(Manuscript received 1 November 1999, in revised form 7 November 2000)

Abstract

In this study, predictability for the barotropic component of the atmosphere is examined based on analog weather maps in the historical data. The limit of predictability P is defined as the time taken for the initial error to reach the climate noise level which is defined by one standard deviation from the long term mean of the fluctuation in the observed atmosphere. According to the quadratic error growth model by Lorenz (1982), the predictability P is expected to obey a logarithmic function rather than a linear function of the initial error. Although we searched 15,667,760 combinations of weather maps, there are no good analog pairs to investigate the error growth for a sufficiently small initial error. For this reason, model experiments were conducted to demonstrate that the quadratic error growth model is applicable to infer the behavior of a small error from the distribution of a large error. From the results of the model experiments, and the best analog pairs in the historical data, we estimated that the predictability for the real atmosphere increases about 6.3 days when the initial error energy is reduced to 1/10. Hence, we may extend the predictability for the barotropic component of the atmosphere if we can reduce the initial error in the vertical mean of the atmosphere.

1. Introduction

In the 1990's, medium-range forecasting by the ensemble mean has been carried out at some operational weather forecasting centers. While the forecasting skill has steadily increased and the range of skillful forecasts has been steadily extended, it has also been established that deterministic prediction of the instantaneous state of the weather is impossible for an extended range. This limit of predictability was first pointed out by Lorenz (1963) who subsequently demonstrated that, due to the inherent nature of instability and nonlinearity, atmospheric flows with only slightly different initial states will depart from each other and evolve eventually to flows that are just randomly related. It is our contention that deterministic medium-range forecasting may be impossible beyond two weeks of the chaotic barrier, even if we can have a perfect prediction model.

Previous studies of the limit of predictability are divided into two groups; one with empirical approach using analog pairs in the historical data and the other with dynamical approach using numerical model experiments (Lorenz 1969a). The empirical approach estimates the predictability of the observed atmosphere based on the growth rate of the difference between the two analog weather maps (e.g., Lorenz 1969b; Gutzler and Shukla 1984). Although Lorenz (1969b) could not find good analog pairs, he indicated that the small error would be double in about 2.5 days. Similar to Lorenz's approach, Gutzler and Shukla (1984) estimated the doubling time as nearly 8 days. It is difficult, however, to estimate the predictability for small error using this approach because it is highly improbable that the truly good analog pair will be found in the historical data (van den Dool 1994).

On the other hand, the dynamical approach estimates the predictability with "identical twin" experiments in which two integrations started from slightly different initial conditions and diverge from

Corresponding author: Hiroshi L. Tanaka, Institute of Geoscience, University of Tsukuba, 1-1-1 Tennoudai, Tsukuba 305-8571, Japan.
E-mail: tanaka@atm.geo.tsukuba.ac.jp

each other, providing information about the limit of predictability (e.g., Lorenz 1982; Dalcher and Kalnay 1987; Schubert and Suarez 1989; Chen 1989; Simons et al. 1995). Lorenz (1982) estimated a doubling time for small errors of only 2.4 days, using a quadratic error growth model constructed from the growth of rms (root mean square) difference in 500 hPa geopotential height between two forecasts. With the same approach, the doubling time for the recent forecast model developed by ECMWF appears to be around 1.5 days (Simons et al. 1995). Dalcher and Kalnay (1987), however, pointed out that the doubling time of small error is not a good measure of the error growth because the result is very sensitive for small error to the error growth model. Therefore, they defined the limit of predictability as the time taken for the error to reach 95% of the climatological mean range of fluctuation in 500 hPa geopotential height, and found the limit of predictability is close to 20 days in winter. In a similar way as Dalcher and Kalnay (1987), Chen (1989) adopted the limit of predictability as the time taken for the error to reach one standard deviation from the climatological mean range of fluctuation, and found the limit of predictability is about 14 days without using the Lorenz's error growth model. However, in order to extrapolate his result to the small initial error, Chen (1989) assumed a linear relationship between the initial error and the limit of predictability. Such a linear relationship was used further by Toth (1991) in a study of predictability based on circulation analogues. From those experiments, it was concluded that the limit of predictability is of the order of two weeks.

For the purpose of extending the limit of predictability, an ensemble of numerical forecasts from slightly perturbed initial conditions was often used for the medium range forecasts at some operational weather forecasting centers (e.g., Molteni et al. 1996; Toth and Kalnay 1997). On the other hand, Miyakoda et al. (1986) constructed a one-month prediction model which predicts the 5-day or 10-day mean field by separating slowly moving low-frequency variability from unpredictable high-frequency eddies. It is hoped, therefore, that some averaged physical quantity may extend the limit of predictability. According to Tanaka and Nohara (2000), a barotropic model developed by Tanaka (1998), which predicts vertical mean state, had a predictability beyond two weeks for the model atmosphere. It may therefore be interesting to pursue the limit of predictability for the barotropic component of the observed atmosphere.

The purpose of this study is to estimate the predictability for the barotropic component of the observed atmosphere using empirical and dynamical approaches. Since the barotropic component of the atmosphere includes much low-frequency components, we may expect a longer upper bound of predictability for the observed atmosphere. In this study, our approach is described as follows. First, we seek for good analog pairs for the barotropic component of the observed atmosphere using the historical dataset of NCEP/NCAR reanalysis. From the behavior of the difference in the good analog pairs, we may estimate the predictability of the barotropic component of the observed atmosphere. As in Lorenz (1969b), Gulzler and Shukula (1984), and van den Dool (1994), such a good analog pair, however, may not be found. Therefore, in the second, we use a barotropic model in order to discuss the behavior of the small error in the model atmosphere.

Although the growth in the difference for the analog pairs is measured for the barotropic components, the growth may be largely affected by the baroclinic-barotropic interactions. Therefore, the examination of the predictability of the barotropic component of the observed atmosphere implicitly includes the influence from the baroclinic components. Yet, for simplicity, we will call it the predictability of the barotropic component of the real atmosphere.

In Section 2, the dataset and analysis method are described. In Section 3, results of the limit of predictability for the observed atmosphere are presented as a function of the initial error. In Section 4, the same results are presented for the model atmosphere. Concluding remarks are given in Section 5.

2. Data and analysis scheme

The data used in this study is NCEP/NCAR reanalysis (Kalnay et al. 1996). The dataset contains four times daily meteorological variables of horizontal wind vector (u, v) and geopotential ϕ at 2.5° longitude by 2.5° latitude grids on 17 mandatory vertical levels of 1000, 925, 850, 700, 600, 500, 400, 300, 250, 200, 150, 100, 70, 50, 30, 20, 10 hPa for 17 years from January 1979 to December 1995. The data at the grid points are transformed into normal mode expansion coefficients in order to reduce the degree of freedom. The normal mode expansion is

described in detail by Tanaka and Kimura (1996), and a brief description is presented here.

A system of primitive equations of the atmosphere with a spherical coordinate may be reduced to three prognostic equations of horizontal motions and thermodynamics for three dependent variables of $\mathbf{U} = (u, v, \phi)^T$. Here, u and v are zonal and meridional components of horizontal velocity. The variable ϕ is a departure of local isobaric geopotential from the global mean reference state, and the superscript T denotes a transpose. Using a matrix notation, these primitive equations may be written as

$$\mathbf{M}\frac{\partial \mathbf{U}}{\partial t} + \mathbf{L}\mathbf{U} = \mathbf{N} + \mathbf{F}. \quad (1)$$

Here, t is time, and the left-hand side represents linear terms with matrix operators $\mathbf{M}$ and $\mathbf{L}$ and the dependent variable vector $\mathbf{U}$. The right-hand side represents a nonlinear term vector $\mathbf{N}$ and a diabatic term vector $\mathbf{F}$, which includes zonal and meridional components of frictional force and a diabatic heating rate.

In order to obtain a system of spectral primitive equations, we expand the vectors $\mathbf{U}$ and $\mathbf{F}$ in 3-D normal mode functions in a resting atmosphere,

$$\Pi_{nlm}(\lambda, \theta, p):$$

$$\mathbf{U}(\lambda, \theta, p, t) = \sum_{n=-N}^{N} \sum_{l=0}^{L} \sum_{m=0}^{M} w_{nlm}(t) X_m \Pi_{nlm}(\lambda, \theta, p), \quad (2)$$

$$\mathbf{F}(\lambda, \theta, p, t) = \sum_{n=-N}^{N} \sum_{l=0}^{L} \sum_{m=0}^{M} f_{nlm}(t) Y_m \Pi_{nlm}(\lambda, \theta, p), \quad (3)$$

where X_m and Y_m are scale matrices. Here, the expansion coefficients $w_{nlm}(t)$ and $f_{nlm}(t)$ are functions of time alone. The subscripts represent zonal wavenumbers n, meridional indices l, and vertical indices m. They are truncated at $\mathbf{N}$, $\mathbf{L}$, and $\mathbf{M}$, respectively. The vertical indices $m = 0$ and $m \neq 0$ represent barotropic and baroclinic modes, respectively.

The 3-D normal mode functions are given by a tensor product of vertical structure functions (vertical normal modes) and Hough harmonics (horizontal normal modes) associated with the linear operators $\mathbf{M}$ and $\mathbf{L}$, respectively. It is known that they form a complete set and satisfy an orthonormality condition under an inner product $\langle \ , \ \rangle$ defined as:

$$\langle \Pi_{nlm}, \Pi_{n'l'm'} \rangle = \frac{1}{2\pi p_s} \int_0^{p_s} \int_{-\frac{\pi}{2}}^{\frac{\pi}{2}} \int_0^{2\pi} \Pi^*_{nlm} \Pi_{n'l'm'} \cos\theta \, d\lambda \, d\theta \, dp = \delta_{nn'} \delta_{ll'} \delta_{mm'}, \quad (4)$$

where the asterisk denotes the complex conjugate, the symbols δ_{ij} is the Kronecker delta, and the surface pressure p_s is treated as a constant near the earth's surface (see Kasahara and Puri 1981). Based on the orthonormality condition, the normal mode expansion coefficients w_{nlm} may be obtained by the following inner product:

$$w_{nlm}(t) = \langle \mathbf{U}, X_m^{-1} \Pi_{nlm} \rangle. \quad (5)$$

Using Eq.(5), we can transform the NCEP/NCAR reanalysis dataset into the normal mode expansion coefficients w_{nlm} for $n = 0 \sim 20$, $l = 0 \sim 20$, and $m = 0$. Here, $m = 0$ means the barotropic component, and only Rossby modes are retained. Only the Northern Hemisphere data are used by the symmetric extension to the Southern Hemisphere.

The total energy E_T (the sum of kinetic energy and available potential energy) for a component of the normal mode expansion may be written as:

$$E_T = \frac{1}{2} p_s h_0 \sum_n \sum_l |w_{nl0}|^2, \quad (6)$$

where p_s is a constant surface pressure (= 1013 hPa), and h_0 is an equivalent depth of the atmosphere (= 9728 m). The total energy E_T has physical units of Jm^{-2}. During winter, the average of E_T is about $1,700 \times 10^3$ Jm^{-2}.

Using the method of the normal mode expansion, we define error energy as a magnitude of the difference between two weather maps (Tanaka et al. 1989). When normal mode expansion coefficients for two maps A and B are denoted as $w_{nl0}(A)$ and $w_{nl0}(B)$, the error energy (E) between the maps is defined as:

$$E[B - A] = \frac{1}{2} p_s h_0 \sum_n \sum_l |w_{nl0}(B) - w_{nl0}(A)|^2. \quad (7)$$

The same dimensional factor as (6) is used, so that E has physical units of Jm^{-2}. The rms difference in the 500 hPa geopotential height has been assessed for the analog weather maps in previous studies. It is considered that the error index E is superior to the rms because E has the same form as total

energy which considers the differences in variables u, v, and ϕ. The best analog pair of maps A and B by this criterion is that it minimizes E in all combinations of the historical data.

3. Growth of error energy for the observed atmosphere

In this section, we focus on the time series of the error energy between two barotropic weather maps for the best analog pair. One thing we need to mention here is that the error growth for the barotropic component of the observed atmosphere contains the influence of that from the baroclinic component of the observed atmosphere. The contribution from the baroclinic component appears as if it is a systematic external forcing, which has no relation to the state variables of the barotropic component of the atmosphere. Therefore, such an external forcing is unpredictable from the barotropic component.

In order to estimate the limit of predictability for the barotropic component of the observed atmosphere, we need to first find the best analog pairs in the past, then analyze the time series of the increasing difference between the two weather maps. When the difference is sufficiently small, it would necessarily grow as the time proceeds. Therefore, the key to the successful analysis for discussing the error growth is to search for sufficiently good analog pairs. Although a similar approach was attempted by Lorenz (1969b), Gutzler and Shukla (1984), and Toth (1991), they failed to determine the limit of predictability since they could not find such good analog pairs for certain pressure levels. Based on their studies, we attempted in this study to seek for analog pairs for the vertical mean component of the atmosphere, using the normal mode expansion. Since the degree of freedom in the state variable is sufficiently small, we can compare more historical data than in previous studies.

In this study, we analyze the dataset for the months of December, January and February — a total of 6012 maps during the 17 years. First, we calculate E in (7) for all combinations of all weather maps. Following Gutzler and Shukla (1984), every weather map for a single winter is compared with all maps of other winters. This procedure is followed to ensure that a good analog pair is not merely due to persistence, but actually represent a recurrence of a circulation pattern. The total number of combinations compared by this procedure, 15,667,760, is much larger than that in Gutzler's study.

Figure 1 illustrates the frequency distribution of E resulted from all combinations of weather maps. We note that the smallest value encountered by this method is 393×10^3 Jm^{-2}. Only two cases are detected from 300×10^3 to 400×10^3 Jm^{-2}. The frequency peak is seen over $1,000 \times 10^3$ to $1,100 \times 10^3$ Jm^{-2} with 2,931,157 cases, and the average E for all combinations is $1,083 \times 10^3$ Jm^{-2}. This value corresponds to the expected value of the difference between two randomly chosen weather maps. It is found that the best analog pair is about half the average value of E. The standard deviation is 213×10^3 Jm^{-2}, with a larger spread in the higher values. Only 15.7% of the samples in all combinations are less than one standard deviation from the mean. From this result, we find it extremely difficult to get a very good analog pair with current observation error (about 20×10^3 Jm^{-2} or 10 m of rms), even though the magnitude of the dataset has dramatically increased. From other method, van den Dool (1994) showed that it was necessary to take a historical data library of the order 10^{30} years in order to find two observed flows that match within the current observation error over the Northern Hemisphere. Therefore, it is difficult to determine the limit of predictability by this method alone.

Table 1 contains a sample list of the best ten independent analog pairs. Because some flow pat-

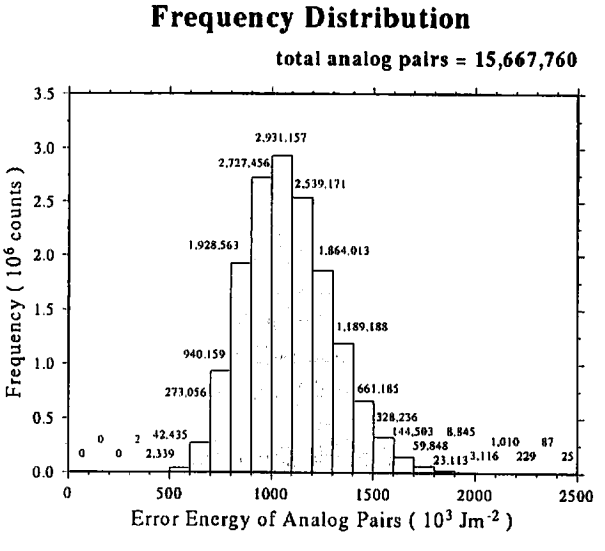

Fig. 1. Frequency distribution of E of all pairs. The total number of the analog pairs is 15,667,760, and the number on the column shows count of each analogous level.

terns persist one day or more, many of the best analog pairs are chosen from the same synoptic situation with one or two days apart. Following Gutzler and Shukla (1984), the dependent analog pairs are subjectively removed by examining the list of the best analog pairs.

Table 1. The list of the best ten independent analog pairs. The first two digits in each date represent the year; the second two digits represent the month; the third two digits represent the day; the last two digits represent the hour (e.g., 8312100 means 0000 Z 10 December 1983).

	Dates of the pair	Error energy $\times 10^3$ J m^{-2}
1	83121000 - 86010312	393
2	80021612 - 86021218	405
3	84012418 - 88021206	405
4	91121118 - 92122312	416
5	87011806 - 90010400	417
6	80122112 - 88020718	424
7	84021018 - 86122318	426
8	88020906 - 91010718	430
9	80022206 - 92012206	430
10	82021518 - 91020218	436
	mean error energy =	1,083

The similarity of the best analog pair can be confirmed visually. Figure 2 illustrates barotropic geopotential heights of the best analog pair in the Northern Hemisphere at 0000Z 10 December 1983 (designated as 83121000), 1200Z 3 January 1986 (86010312), and their difference. The contour interval is 60 m. Since the geopotential height is defined as a deviation from the global mean reference state, the contours are positive for low latitudes and negative for high latitudes. This pair is very similar over the middle latitude, but not over the Arctic. The figure shows that the difference in the geopotential height is at most 240 m over Siberia, and E over the Hemisphere is 393×10^3 Jm^{-2}. The error energy E of this pair gradually increases as time proceeds.

Figure 3 illustrates time variation of E (solid curve) for 10 days from the date of the best analog pair. The heavy and thin straight lines represent the climatological mean of fluctuation (about $1,083 \times 10^3$ Jm^{-2}) and the one standard deviation from the mean (about 870×10^3 Jm^{-2}) in the observed atmosphere, respectively. Hereafter, we refer to this range as a noise range. The error energy E increases exponentially for 0–3 days. When E reaches the noise range, it may be no longer considered as an analog pair. For the analogy in weather prediction, it may be the criterion that the predictability is lost. For this reason, we define a

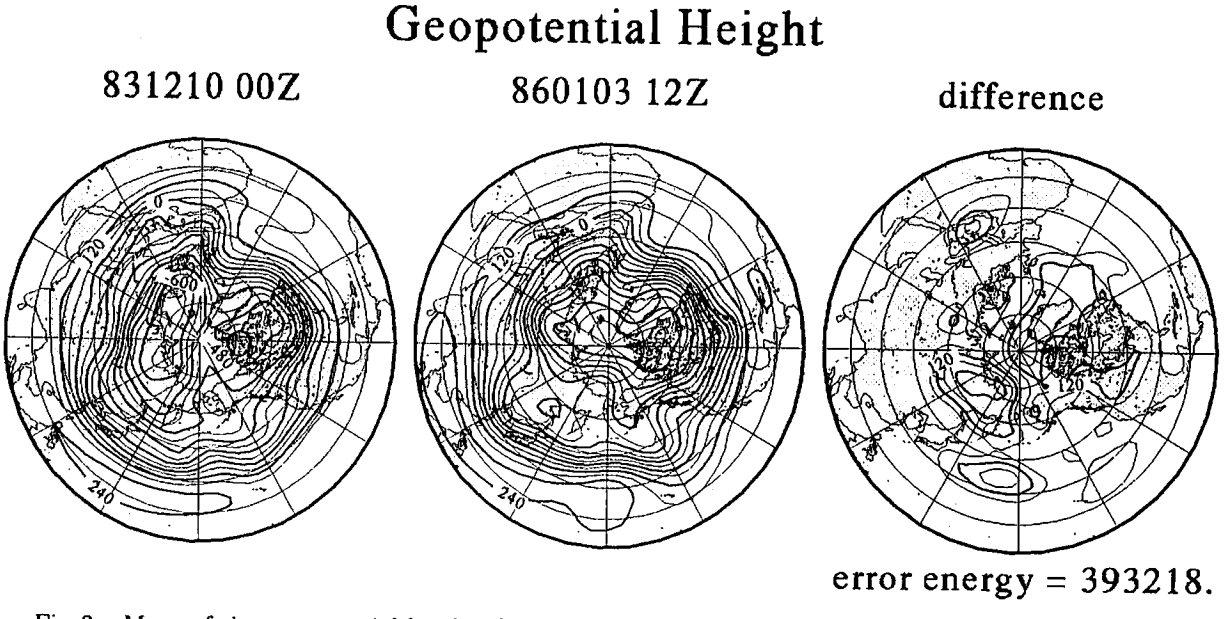

Fig. 2. Maps of the geopotential height. Shown are the best analog pairs for 0000Z 10 December 1983 (left), 1200Z 3 January 1986 (middle), and their difference (right). Contour interval is 60 m.

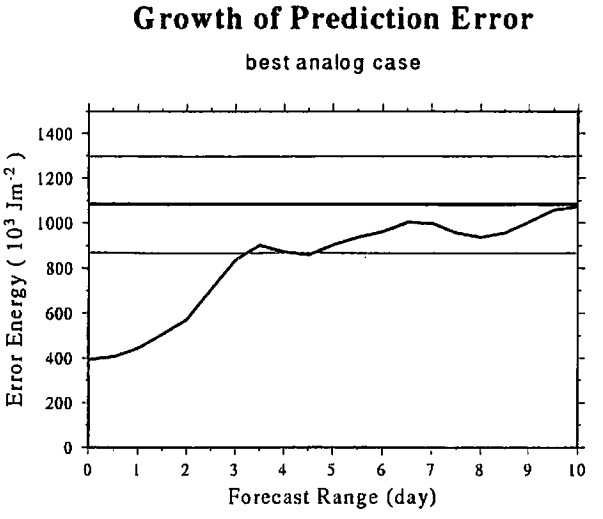

Fig. 3. Time variation of E. The solid curve represents the E for the best analog pair. The heavy and thin straight lines represent the climatological mean range of fluctuation (about $1,083 \times 10^3$ Jm^{-2}) and the one standard deviation from the mean (about 870×10^3 Jm^{-2}) in the observed atmosphere, respectively.

limit of predictability (designated as P) as the time taken for E to reach the noise range. In this case, P for the best analog pair is about 3 days.

In order to expect higher accuracy in the predictability of the atmosphere, we calculated the average of the best 50 analog pairs to measure the predictability P. Figure 4 illustrates time variations of E for the best 50 individual analog pairs

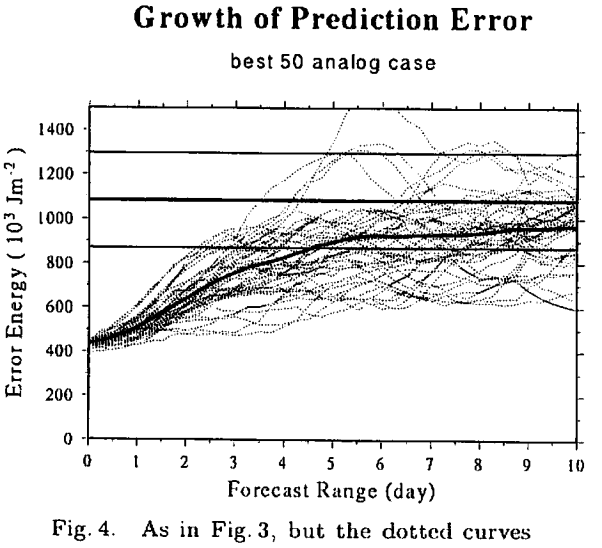

Fig. 4. As in Fig. 3, but the dotted curves represent the individual E for the best 50 analog pairs and solid curve represents the average.

(dotted curve), and the average (solid curve). The most rapid event of the error growth reaches the noise range at 2.5 days. In contrast, the slowest cases reach the noise range after 10 days. The average of E reaches the noise range at 4.5 days. Accordingly, the predictability P for the average of the best 50 analog pairs is about 4.5 days when the initial error energy (designated as E_0) is about 430×10^3 Jm^{-2}.

Similar to the solid curve in Fig. 4, the error growth for various magnitudes of E_0 are calculated. Figure 5 illustrates the scatter diagram of P as a function of E_0 in reference to Chen (1989). A linear regression between E_0 and P yields:

$$P = -1.03 \times 10^{-5} E_0 + 10.2. \quad (8)$$

The correlation coefficient is -0.86. This intercept means that if there is a very good analog pair in which E is almost 0 Jm^{-2}, the predictability P is 10.2 days. The predictability for the barotropic component would have an upper bound if the relationship lays on a linear line. The predictability P would be 10.2 days for an infinitesimal initial difference in the observed atmosphere.

We consider a logarithmic function for the fitting function based on a quadratic error growth model

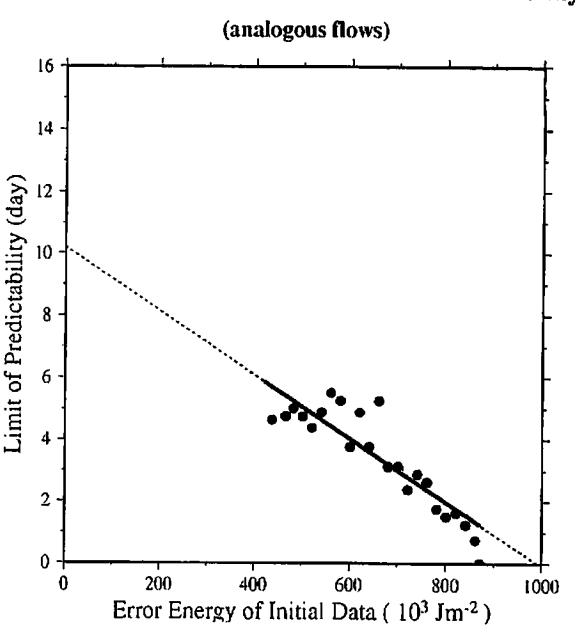

Fig. 5. Scatter diagram of the E_0 against P in the observed atmosphere. The solid line is the best fit of linear regression of those solid circles and the dashed line is the extrapolation of the solid line.

(Lorenz 1969b; Lorenz 1982; Stroe and Royer 1993). The error growth model is written as

$$\frac{dE}{dt} = \alpha E - \frac{\alpha}{E_\infty} E^2, \quad (9)$$

where E_∞ is a saturated error value (equal to the climatological mean of the fluctuation). The equation allows an exponential growth of error with a growth rate given by α for small differences, and the error will saturate at a sufficiently long time. In previous studies, the error growth was fit on this equation to obtain α. However, it is difficult to fit the relation between dE/dt and E for a small error because the term dE/dt is very sensitive to compute in differential form. We thus attempted to fit the error growth on the integrated form of (9).

The integral form of this equation is given by Stroe and Royer (1993) as

$$E = \frac{E_\infty}{1 + \left(\frac{E_\infty}{E_0} - 1\right) e^{-\alpha t}}. \quad (10)$$

Eq.(10) may be written for P using E_0 as

$$P = -\frac{1}{\alpha}\left\{\log\left[\frac{E_0}{E_\infty - E_0}\right] + \log\left[\frac{E_\infty - E_l}{E_l}\right]\right\}, \quad (11)$$

where E_l is the error energy at $t = P$. If E_0 is closed to 0, then the relation between P and E_0 will be logarithmic.

Figure 6 illustrates the same scatter diagram as in Fig. 5, but with a logarithmic scale in E_0 and the fitting curve using (11) for E_l. The regression between E_0 and P yields:

$$P = -6.3 \log_{10}\left(\frac{E_0}{E_\infty - E_0}\right) + 3.8. \quad (12)$$

This equation means that the limit of predictability P extends 6.3 days when E_0 is reduced to 1/10 for sufficiently small E_0 (the corresponding error e-folding time is 5.4 days). The predictability for the barotropic component would be unbounded for the limit as E_0 approaches 0 if the relationship lays on a logarithmic line. In this case, we can extend the predictability as long as we can reduce the initial error.

However, we can not conclude whether the predictability is bounded or unbounded since E_0 in the observed atmosphere is too large even for the best analog pair to assess the features of the small range of error energy. We will discuss this problem using a barotropic model in the next section.

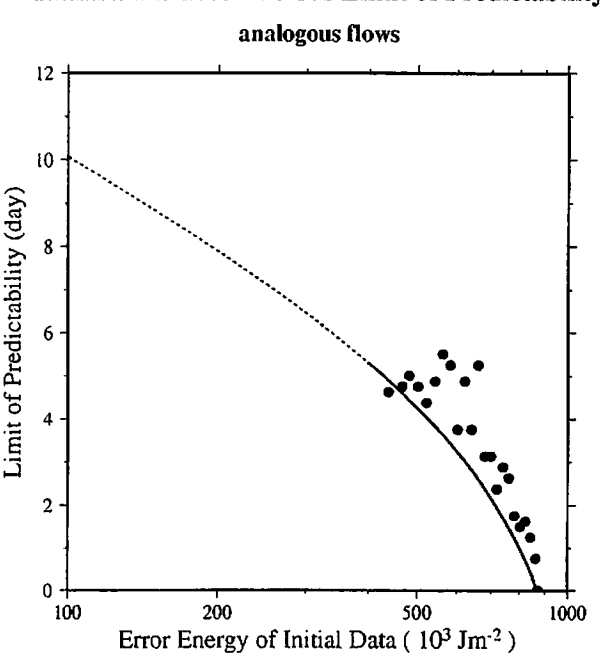

Fig. 6. Same as Fig. 5, but with a logarithmic scale in E_0 and the regression using the quadratic error growth model.

4. Growth of error energy for model atmosphere

In this section, we focus on a behavior of the small initial error using a barotropic model developed by Tanaka (1991; 1998) for Monte Carlo experiments. Even with a perfect model, a slight initial difference would grow as time goes due to the dynamical instability and nonlinearity. We can thus estimate the predictability for the model atmosphere from the behavior of the small initial error. A detailed description of the model is provided by Tanaka (1991; 1998), so only a brief description is presented here.

Applied the inner product (4) to the system of spectral primitive equations (1), the weak form of the equation becomes

$$\left\langle \mathbf{M}\frac{\partial \mathbf{U}}{\partial t} + \mathbf{LU} - \mathbf{N} - \mathbf{F}, Y_m^{-1}\Pi_{nlm} \right\rangle = 0. \quad (13)$$

Substituting (2) and (3) into (13), rearranging the time-dependent variables, and evaluating the remaining terms, we obtain a system of 3–D spectral primitive equations in terms of the spectral expansion coefficients:

$$\frac{dw_i}{d\tau} + i\sigma_i w_i = -i\sum_{jk} r_{ijk} w_j w_k + f_i,$$
$$i = 1, 2, 3, \cdots \quad (14)$$

where τ is a dimensionless time scaled by 2Ω, σ_i is the eigenfrequency of the Laplace's tidal equation, and r_{ijk} is the interaction coefficients for nonlinear wave-wave interactions. The triple subscripts are shortened for simplicity as $w_{nlm} = w_i$. There should be no confusion in the use of i for a subscript even though it is used for the imaginary unit.

In the 3-D spectral primitive equations, the vertical expansion basis functions may be divided into barotropic and baroclinic components. We may construct a simple spectral barotropic model, using only the barotropic components of the Rossby modes, by truncating all the baroclinic modes and high-frequency gravity modes (see Kasahara 1977):

$$\frac{dw_i}{d\tau} + i\sigma_i w_i = -i\sum_{jk} r_{ijk} w_j w_k + f_i,$$
$$i = 1, 2, 3, \cdots, \qquad (m = 0), \quad (15)$$

where the indices of the subscripts run only for the barotropic modes ($m = 0$), and the zonal and meridional wave truncation is equivalent to rhomboidal 20 with an equatorial wall. In this study, we consider only the following five physical processes:

$$f_i = (BC)_i + (TF)_i + (DF)_i + (DZ)_i + (DE)_i, \quad (16)$$

where $(BC)_i$ represents the baroclinic instability, $(TF)_i$ the topographic forcing, $(DF)_i$ the biharmonic diffusion, $(DZ)_i$ the zonal surface stress, and $(DE)_i$ the Ekman pumping for eddies. Apart from the energy source of the $(TF)_i$, the sole energy source of the model is $(BC)_i$ induced by the barotropic-baroclinic interaction. The rest of the three physical processes are the energy sinks of this model. Refer to Tanaka (1991; 1998) for more comprehensive description of these forcing.

Using the barotropic model, a perpetual winter time integration is conducted as a control run for 600 days. The initial state is an axisymmetric flow. Disturbances are soon excited by topographic forcing, and the eddy is saturated at an equilibrium energy level about 70 days after the time integration. Some pronounced blockings appear repeatedly in the model atmosphere, especially over the North Pacific and North Atlantic sections.

Next we integrate 50 test runs for 300 days with initial conditions of contiguous each 5 days during 255 to 500 days in the control run. A very small white noise (0.05% of the total energy) is superimposed on each initial data to examine the growth of the initial error. Figure 7 shows individual E of 50 test runs (dotted curve). The heavy and thin straight lines represent the climatological mean of

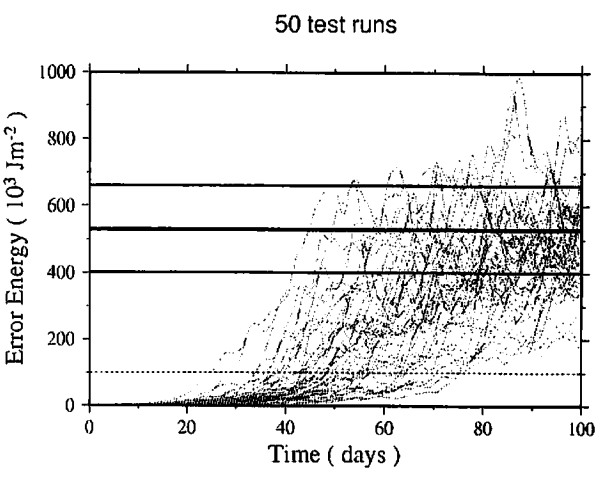

Fig. 7. Time variation of E. The dotted curves represent the individual E for the 50 test runs. The heavy and thin straight lines represent the climatological mean of the fluctuation and its one standard deviation from the mean in the model atmosphere. The dotted straight line represents a specified error level E_0 (100×10^3 Jm^{-2}).

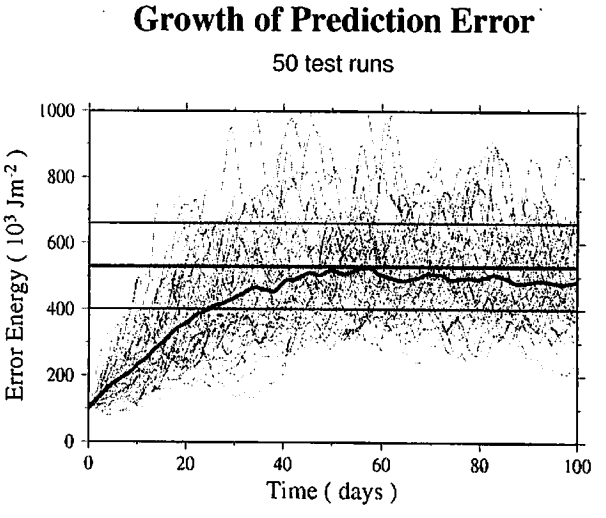

Fig. 8. Same as Fig. 7, but individual E of the test run (dotted curve) and the average (solid curve) started from these structures of the error at the error energy level of 100×10^3 Jm^{-2} in Fig. 7.

the fluctuation and its one standard deviation from the mean in the model atmosphere.

The error growth for the white noise depends on the background flow and the structure of white noise. We often observe an initial decrease of E to adjust the background flow. For this reason, we let the very small error grow to a specified error level E_0 (100×10^3 Jm^{-2} in Fig. 7) and use the structure of the error for the next test run.

Figure 8 shows individual E of the test run (dotted curve) and the average (solid curve) started from these structures of the error at the error energy level of 100×10^3 Jm^{-2} in Fig. 7. The limit of predictability P is defined here as the time taken for the averaged E to reach the one standard deviation in the model atmosphere (about 400×10^3 Jm^{-2}). In this case, the predictability P for the averaged E is about 25 days when the initial error E_0 is 100×10^3 Jm^{-2}.

In order to obtain the relationship between P and E_0, we measure the value of P for various values of E_0 ranging from 1.0×10^3 Jm^{-2} to 400×10^3 Jm^{-2}. Figure 9 illustrates a scatter diagram of P as a function of E_0 in the model atmosphere. As we can clearly see from the Fig. 9, it fits the logarithmic relation between P and E_0. The logarithmic regression using (11) yields:

$$P = -23.7 \log_{10} \left(\frac{E_0}{E_\infty - E_0} \right) + 11.6. \qquad (17)$$

The result implies that the limit of predictability extends 23.7 days when the initial error decreased to 1/10 (20.6 days of error e-folding time) for sufficiently small E_0. The logarithmic relation implies that the predictability for the model atmosphere is unbounded in theory.

To infer the limit of predictability for the real atmosphere from the result of the model, we need to compare the regression using a wide range of E_0 with that using only large E_0, because the real atmosphere offers only large E_0. Figure 10 illustrates the same result as Fig. 9, but with a new dotted regression line calculated only with the large E_0 over 200×10^3 Jm^{-2} (black circles). The logarithmic regression yields:

$$P = -21.2 \log_{10} \left(\frac{E_0}{E_\infty - E_0} \right) + 10.3. \qquad (18)$$

The comparison of (17) and (18) shows that the logarithmic coefficients differ by only 10%. The result suggests that we may infer the predictability for small initial error based on the logarithmic regression using only the large initial error.

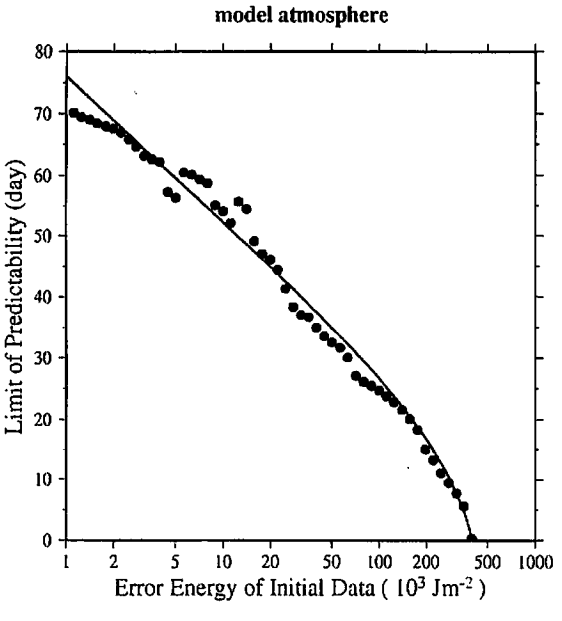

Fig. 9. Scatter diagram of the E_0 against the P in the model atmosphere. The solid line is the regression using the quadratic error growth model.

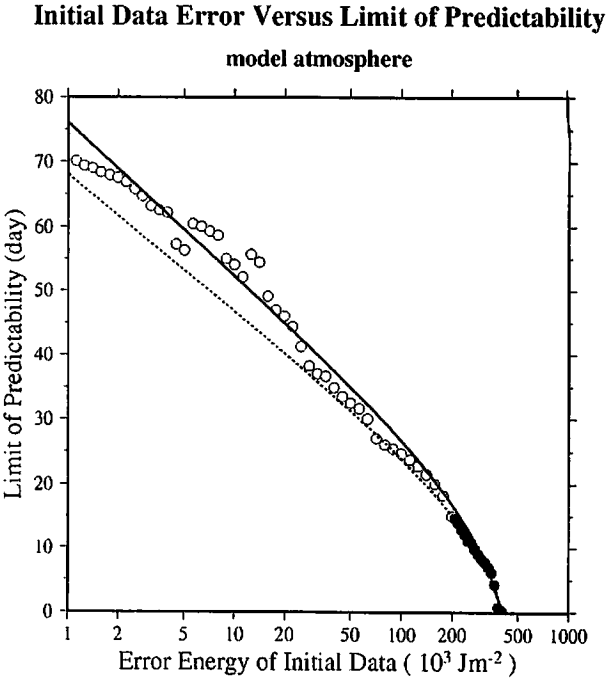

Fig. 10. Same as Fig. 9, but with a new dotted regression line calculated only with the large E_0 over 200×10^3 Jm^{-2} (black circles).

Although it is difficult to discuss the growth of a small error in the observed atmosphere, the behavior of the small error may be estimated from the extrapolation using the result of the model experiments. In a similar study, Toth (1991) estimated the predictability for the real atmosphere using analog weather maps and model atmosphere. He concluded that the relation between E_0 and P fits well on a linear regression, although there was no argument for the behavior of sufficiently small error. On the other hand, we demonstrated in this study that the regression fits well on a logarithmic line rather than the linear line as shown by Toth (1991) for sufficiently a small error. Hence, it is suggested that the predictability of the observed atmosphere also obeys a logarithmic line as in Fig. 6. If this is the case, the limit of predictability extends 6.3 days when the initial error energy decreases to 1/10.

Nevertheless, the error growth rates for the observed and model atmospheres are different from each other. The discrepancy may be explained, first, by the different background conditions with a low-frequency intraseasonal anomaly caused by SST or other external forcings. For example, the analog pairs are not necessarily chosen from the same day of the year. The climatological forcing would be different for the different days of the year, which may result in the faster error growth in the observed atmosphere. Second, the simple external forcing in the model atmosphere compared with the complexity of the real atmosphere may result in a slow error growth. The faster error growth for the observed atmosphere are largely derived by the systematic external forcing from the baroclinic component of the atmosphere which has no relation to the barotropic component. For these reasons, the error growth rate appears to be smaller in the model atmosphere than in the observed atmosphere. However, the true reason for the discrepancy would be reserved for a future work.

5. Conclusion

In this study, we estimated predictability for the barotropic component of the observed atmosphere. The dataset used in this study is the NCEP/NCAR reanalysis. First, we transformed the NCEP/NCAR reanalysis into normal mode expansion coefficients for 17 years (January 1979 to December 1995) using the Northern Hemisphere data. The barotropic components of the Rossby modes are compared to look for analog pairs in the spectral domain. The number of the total combinations of the possible analog pair of weather maps is 15,667,760.

As a result, we found that the average of error energy E in all combinations of all weather maps is $1,083 \times 10^3$ Jm^{-2}. Among those, the best analog pair appears to be 393×10^3 Jm^{-2}; about a half of the average value. The limit of predictability P is then defined as the time taken for the error (i.e., the difference between the two analog maps) to reach the climate noise level defined by the one standard deviation from the climatological mean of the fluctuation in the observed atmosphere (about 870×10^3 Jm^{-2}). If the predictability P is a linear function of the magnitude of the initial error, the result would imply that the predictability is bounded at the limit of vanishing initial error. If this is the case, P becomes 10.2 days. According to the quadratic error growth model by Lorenz (1982), however, the predictability P is expected to obey a logarithmic function rather than the linear function of the initial error. In this case the predictability increases about 6.3 days when the initial error energy reduced to 1/10, implying that P is unbounded in theory.

For the observed atmosphere, however, we could not estimate the limit of predictability because even for the best analog pair, the error is too large to assess the behavior of the growth for small error. This result agrees well with previous studies such as Lorenz (1969b) and Gulzler and Shukula (1984).

In order to infer whether the relationship is linear or logarithmic, we examined this problem using a barotropic model developed by Tanaka (1991; 1998). As a result, it turns out that the relationship is logarithmic in the model atmosphere, suggesting that the predictability is unbounded. It is demonstrated that the limit of predictability increases at about 23.7 days, when the initial error energy was reduced to 1/10 in the model atmosphere. We also demonstrated that the error growth rate could be estimated by using only the large initial error based on the quadratic error growth model.

The result of the logarithmic relation in the model atmosphere is extrapolated to the observed atmosphere. It is concluded in this study that the predictability increases at about 6.3 days when the initial error energy reduced to 1/10 in the observed atmosphere. The corresponding error e-folding time is 5.4 days. Hence, we may extend the predictability for the barotropic component of the atmosphere if we can reduce the initial error for the vertical

mean component of the atmosphere.

Acknowledgments

The authors thank Professor Tetsuzou Yasunari for guidance and advice, and Professor Fujio Kimura for helpful suggestions. It is a pleasure to acknowledge the advice of the members in the climatological and meteorological group in the University of Tsukuba. The authors appreciate Ms. K. Honda for her technical assistance.

References

Chen, W.Y., 1989: Estimate of dynamical predictability from NMC DERF experiments. *Mon. Wea. Rev.*, **117**, 1227–1236.

Dalcher, A. and E. Kalnay, 1987: Error growth and predictability in operational ECMWF forecasts. *Tellus*, **39**, 474–491.

Gutzler, D.S. and J. Shukla, 1984: Analogs in the wintertime 500 mb height field. *J. Atmos. Sci.*, **41**, 177–189.

Kalnay, E., M. Kanamitsu, R. Kistler, W. Collins, D. Deaven, L. Gandin, M. Iredell, S. Saha, G. White, J. Woollen, Y. Zhu, M. Chelliah, W. Ebisuzaki, W. Higgins, J. Janowiak, K.C. Mo, C. Ropelewski, J. Wang, A. Leetmaa, R. Reynolds, R. Jenne and D. Joseph, 1996: The NCEP/NCAR 40-year reanalysis project. *Bull. Amer. Meteor. Soc.*, **77**, 437–471.

Kasahara, A., 1977: Numerical integration of the global barotropic primitive equations with hough harmonic expansions. *J. Atmos. Sci.*, **34**, 687–701.

——— and K. Puri, 1981: Spectral representation of three-dimensional global data by expansion in normal mode functions. *Mon. Wea. Rev.*, **109**, 37–51.

Lorenz, E.N., 1963: Deterministic nonperiodic flow. *J. Atmos. Sci.*, **20**, 130–141.

———, 1969a: Three approachs to atmospheric predictability. *Bull. Amer. Meteor. Soc.*, **50**, 345–349.

———, 1969b: Atmospheric predictability as revealed by naturally occurring analogues. *J. Atmos. Sci.*, **26**, 636–646.

———, 1982: Atmospheric predictability experiments with a large numerical model. *Tellus*, **34**, 505–513.

Miyakoda, K., J. Situtis and J. Ploshay, 1986: One-month forecast experiments-without anomaly boundary forcings. *Mon. Wea. Rev.*, **114**, 2363–2401.

Molteni, F., R. Buizza, T.N. Palmar and T. Petroliagis, 1996: The ECMWF ensemble prediction system: methodology and validation. *Quart. J. Roy. Meteor. Soc.*, **122**, 73–119.

Schubert, S.D. and M. Suarez, 1989: Dynamical predictability in a simple general circulation model: average error growth. *J. Atmos. Sci.*, **46**, 353–370.

Simmons, A.J., R. Mureau and T. Petroliagis, 1995: Error growth and estimates of predictability from the ECMWF forecasting system. *Quart. J. Roy. Meteor. Soc.*, **121**, 1739–1771.

Stroe, R, J.F. Royer, 1993: Comparison of different error growth formulas and predictability estimation in numerical extended-range forecasts. *Ann Geophysicae*, **11**, 296–316.

Tanaka, H.L., 1991: a numerical simulation of amplification of low-frequency planetary waves and blocking formations by the upscale energy cascade. *Mon. Wea. Rev.*, **119**, 2919–2935.

———, 1998: Numerical simulation of a life-cycle of atmosphere blocking and the analysis of potential vorticity using a simple barotropic model. *J. Meteor. Soc. Japan*, **76**, 983–1008.

——— and K. Kimura, 1996: Normal-mode energetics analysis and the intercomparison for the recent ECMWF, NMC, and JMA global analyses. *J. Meteor. Soc. Japan*, **74**, 525–538.

———, E.C. Kung and W.E. Baker, 1989: Nomal mode energetics and error analysis of GLA GCM simulations with different horizontal resolutions during a winter month. *Contribution to Atmospheric Physics*, **62**, 99–111.

——— and D. Nohara, 2001: A study of deterministic predictability for the barotropic component of the atmosphere. *Sci. Rep., Inst. Geosci., Univ. Tsukuba*, (in press).

Toth, Z., 1991: Estimate of atmospheric predictability by circulation analogs. *Mon. Wea. Rev.*, **119**, 65–72.

———, and E. Kalnay, 1997: Ensemble forecasting at NCEP and the breeding method. *Mon. Wea. Rev.*, **125**, 3297–3319.

Van den Dool, H.M., 1994: Searching for analogues, how long must we wait?. *Tellus*, **46A**, 314–324.